Hindawi
Shock and Vibration
Volume 2018, Article ID 9048695, 13 pages
https://doi.org/10.1155/2018/9048695

Research Article

Analysis and Optimization of the Vibration and Noise of a Double Planetary Gear Power Coupling Mechanism

Weijian Zhou, Yanyan Zuo, and Mingyin Zheng

Institute of Noise and Vibration, Jiangsu University, Zhenjiang 212013, China

Correspondence should be addressed to Yanyan Zuo; yyzuo@mail.ujs.edu.cn

Received 12 July 2018; Revised 22 September 2018; Accepted 14 October 2018; Published 15 November 2018

Academic Editor: Adam Glowacz

Copyright © 2018 Weijian Zhou et al. This is an open access article distributed under the Creative Commons Attribution License, which permits unrestricted use, distribution, and reproduction in any medium, provided the original work is properly cited.

As the key component of a hybrid electric vehicle (HEV), the dynamic performance of the power coupling mechanism is found to have a significant effect upon the vibration and noise of the whole vehicle. In this paper, a dynamic model with rigid and flexible bodies of a double planetary gear power coupling mechanism is established. Then, the characteristics of the bearing constraining forces in time domain and frequency domain are simulated and analysed. At the same time, the finite element model of the housing of the power coupling mechanism is established. Then, the vibration response of the housing is analysed under the excitation of the bearing constraining forces, and the vibration displacement of the housing surface is obtained. Furthermore, based on the vibration displacement of the housing surface, a prediction model of housing radiating noise is established. Then, the radiating noise characteristics of the housing and the acoustic contribution of each panel are analysed. Finally, the free damping structure and new stiffener structure are adopted to optimize the rear end cover of the housing. The optimization model based on the vibration acceleration of the rear end cover surface is established by applying K-S function and response surface method. Then, the optimization model is solved by applying the sequential quadratic programming to obtain the optimal structure of the housing. The optimization results demonstrate that the acoustic power level after optimization is decreased by 3.94 dB, 3.92 dB, 5.59 dB, and 2.84 dB at frequencies of 770 Hz, 870 Hz, 1650 Hz, and 2480 Hz, respectively. Therefore, the optimization effect of the housing structure is obvious, and this can be the theoretical basis and reference for reducing the vibration and noise of the power coupling mechanism.

1. Introduction

It is known that the power of HEV is coupled, switched, and output by a power coupling mechanism which is composed of the power coupling system (gear pairs, transmission shafts, bearings, etc.), the structural system (housing), motors, the electrical control system, and other subsystems. As one of the key components of HEV, the dynamic performance of the power coupling mechanism has a great influence on the powertrain and even the whole vehicle [1]. However, since the operating conditions of HEV are complex and changeable, the mode of power coupling mechanism is switched frequently. At the same time, the vibration excitation sources of the power coupling mechanism are complicated, and the excitation frequencies are quite high. Besides, the machining error and unreasonable assembly also need to be considered. Therefore, the vibration and noise of the power coupling mechanism is becoming more and more prominent for HEV [2].

In all types of the power coupling mechanism used in HEV, the double planetary gear power coupling mechanism is widely used because of its properties of small size, light weight, strong bearing capacity, and high transmission efficiency [3]. Planetary gear is widely used in the coupling of hybrid electric vehicles, and its dynamic characteristics directly affect the transmission performance of the coupling mechanism. The dynamic characteristics of gear system, including shock, vibration, and noise in the course of power transmission, are the core of the dynamic research of gear system. According to the difference of the research purpose and the gear transmission system, the dynamic modelling methods of the gear transmission system mainly include the lumped parameter method [4], the finite element method, and the multibody dynamics method. In 1967, Opitz established meshing transmission models of spur gear and helical gear respectively, analysed the influence of transmission error and gear precision on vibration and noise, and

laid the foundation of modern gear dynamics research [5]. In 1993, Kahraman applied lumped parameter method to study the vibration of gear system. The influence of meshing coincidence degree, tooth side clearance, meshing stiffness, and other factors on the dynamic characteristics of gear system was systematically analysed [6–8]. In 2007, Lin et al. established the finite element model of gear system based on the flexibility matrix equation of contact zone, derived the load distribution and meshing stiffness of gear teeth, and analysed the dynamic response of gear system under different instantaneous loads and tooth side clearance. The differences between the contact force of cylindrical gear and that of helical gear are also quantified [9].

At present, the research about HEV is mainly concentrated on the control strategy [10]. However, there are few research studies on the dynamics of the planetary gear power coupling mechanism. Therefore, it is necessary to systematically explore and introduce relevant theories and methods. The paper will present the work on multibody dynamic model, multibody dynamic simulation, vibration response analysis, simulation and analysis of the housing radiating noise, and optimal design of the housing structure. The related work that we have done on the NVH of this double planetary gear power coupling mechanism has not been found in previous research, so it can provide a certain reference for the vibration and noise reduction of the double planetary gear power coupling mechanism.

In this paper, a double planetary gear power coupling mechanism is taken as the research object. Its multibody dynamic model of the power coupling system is established. Then, the characteristics of the bearing constraining forces of the power coupling system in time domain and frequency domain under power switching condition are simulated and analysed. At the same time, the vibration response and radiating noise of the power coupling mechanism housing are analysed. Finally, the optimal design of the housing structure is discussed.

2. Multibody Dynamic Model of the Power Coupling System

The 3D solid model of each component of the power coupling system is built with software UG, and then the assembly model is established [11], as shown in Figure 1. Table 1 below shows the gear parameters of the front planet row and the rear planet row. Table 2 below shows the gear parameters of the first reduction mechanism and the second reduction mechanism.

It can be seen from Figure 1 that the double planetary gear power coupling mechanism is mainly composed of front planet row, rear planet row, composite mechanism, motor MG1, motor MG2, first reduction mechanism, and second reduction mechanism. The working principle is as follows: the front planet row is used for power distribution, and the rear planet row is used to reduce the speed. The engine is connected to the planet carrier of the front planet row by torsional shock absorbers, and the motor MG1 is connected to the sun gear of the front planet row. At the same time, the motor MG2 is connected to the sun gear of the rear planet row, and the planet carrier of the rear planet row is fixed on the outer shell. By applying different speed and torque to engine, motor MG1 and motor MG2, the different working conditions of the hybrid electric vehicle can be realized, including the pure electric drive condition, engine starting under the pure electric drive condition, low-speed cruising condition, high-speed cruising condition and so on. The power is eventually output to the first and second reduction mechanisms through the outer gear ring of the composite mechanism and then to vehicle wheels.

After the solid modelling in software UG, the solid model of the power coupling system is input into the software ADAMS in which the material properties of each component of the system are defined. In order to define the motion relationships among the components, the constraint relation is applied, including revolute joints and fixed joints. The constraint relation is as follows: firstly, the engine input shaft, rotor of motor MG1, rotor of motor MG2, composite mechanism, first reduction gear shaft, and second reduction gear shaft are connected to the ground separately with revolute joints. The planet gears of the front planet row are connected to the planet carrier separately with revolute joints. The planet gears of the rear planet row are connected to the planet carrier separately with revolute joints. Secondly, the engine input shaft is connected to the planet carrier of the front planet row with a fixed joint. The rotor of motor MG1 and the sun gear of the front planet row are connected to the MG1 input shaft separately with fixed joints. The rotor of motor MG2 and the sun gear of the rear planet row are connected to the MG2 input shaft separately with fixed joints. The planet carrier of the rear planet row is connected to the ground with a fixed joint. The internal gear ring of the front planet row, the internal gear ring of the rear planet row, and the outer gear ring of the composite mechanism are connected to the composite mechanism separately with fixed joints.

At the same time, the contact parameters of the gear pairs are defined. In addition, since the input shafts from the engine and two motors are prone to elastic deformation, they are treated as flexible bodies [12]. Finally, the dynamic model with rigid and flexible components of the power coupling system is established in software ADAMS, as shown in Figure 2.

Due to the lack of the experiment bench, all the results obtained in the following sections are from simulation using commercial software. In order to make sure the correctness of model, the solid model of the double planetary gear power coupling mechanism has been accurately established in software UG. In addition, the material properties and constraint relation has been accurately defined in software ADAMS. Since the input shafts from the engine and two motors are prone to elastic deformation, they are treated as flexible bodies in software ADAMS. Therefore, the error of the model is already very small, and all the simulation results should be reliable.

3. Multibody Dynamic Simulation of the Power Coupling System

3.1. Selection of the Simulation Condition. Road tests are done on HEV, and Table 3 illustrates the working conditions of

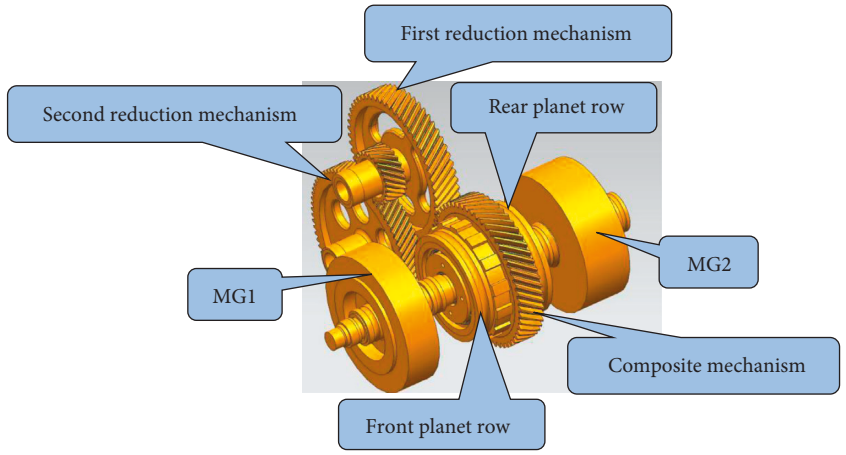

Figure 1: Assembly model of the power coupling system.

Table 1: Gear parameters of the front and rear planet rows.

Parameters	Front planet row			Rear planet row		
	Sun	Planets	Internal gear	Sun	Planets	Internal gear
Tooth number	30	23	78	22	18	58
Face width (mm)	27.5	25	25	50	35	35
Direction	Left	Right	Right	Left	Right	Right
Module (mm)	1			1.5		
Pressure angle	20°			20°		
Helix angle	25°			30°		

Table 2: Gear parameters of the first and second reduction mechanisms.

Parameters	First reduction mechanism		Second reduction mechanism	
	Driving gear	Driven gear	Driving gear	Driven gear
Tooth number	54	55	24	77
Face width (mm)	30	30	25	25
Direction	Right	Left	Right	Left
Module (mm)	2.5		2	
Pressure angle	20°		20°	
Helix angle	30°		30°	

HEV and the data obtained in road tests, including the engine speed and torque, the motor speed and torque, and the battery data.

It is known that the engine needs to start and stop frequently during the operation of HEV, especially when the pure electric drive mode is switched to the combined drive mode of engine and motor, the vibration and noise caused by transient impact from power switching is particularly obvious. Therefore, the dynamic characteristics of power coupling system are analysed by choosing the power switching mode of the HEV as the simulation condition, during which the engine starts under the pure electric drive condition.

3.2. Dynamic Simulation and Analysis under the Chosen Condition. According to the data in Table 3, the operating condition where the engine starts under pure electric drive condition is simulated in software ADAMS. The load torque applied on the power output shaft of the reduction gear assembly is 55071 N·mm. From 0.05 s to 0.25 s, the speed of motor MG1 is changed from 13308 d/s (in forward direction) to −3972 d/s (in reverse direction). Meanwhile, the speed of motor MG2 is 13500 d/s (in positive direction). The load torque applied on the engine shaft is 34000 N·mm. The duration of simulation is 0.25 s, and step length is 0.0001 s. The simulation results of the bearing constraining forces of the power coupling system are shown in Figure 3. The bearing force in Figure 3 is a resultant force which can be decomposed into the component forces in X, Y, and Z directions. The X and Z directions point to the radial direction of the bearing, and the Y direction points to the axial direction of the bearing. The direction of the resultant force is determined by three component forces in X, Y, and Z directions.

As the vibration excitation sources of housing, bearing constraining forces directly affect the vibration and radiating noise of the power coupling mechanism. Therefore, it is necessary to analyse the time histories and frequency spectra of bearing constraining forces. The related analysis is as follows.

From Figures 3(a) and 3(b), it can be seen that in the initial stage of power switching, both the engine input shaft bearing and the MG1 input shaft bearing have transient impact, but after the engine starts, the time domain signals of their bearing constraining forces are gradually stable.

It is known that the composite mechanism needs to not only couple the speed and torque of the power sources, but also bear the transient impact generated when the power of

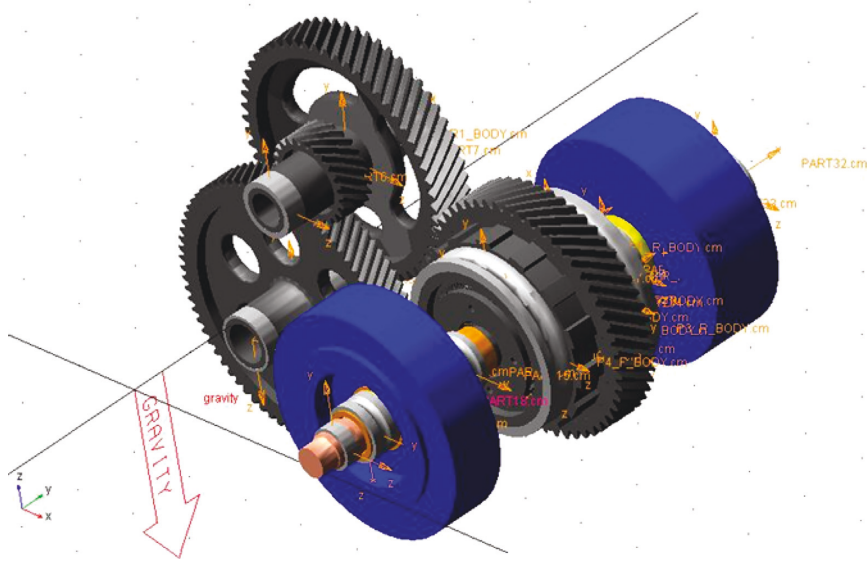

Figure 2: Dynamic model with rigid and flexible components.

Table 3: Data obtained in road tests.

Working conditions	v (km/h)	n_{ENG} (r/min)	n_{MG2} (r/min)	T_{MG2} (N·m)	n_{MG1} (r/min)	T_{MG1} (N·m)	SOC (%)
Pure electric drive condition	30	0	2250	16.75	−2220	0	49.5
Engine starts under the pure electric drive condition	30	0~800	2250	45~8	−2218~662	0~27.6	47
Low-speed cruising condition	30	1220	2205	−9.25	2247	−6.25	45
High-speed cruising condition	80	1408	6010	−9.95	−923	−20.1	51.3

Note. v is the vehicle speed, n_{ENG} is the engine speed, n_{MG2} is the speed of motor MG2, T_{MG2} is the torque of motor MG2, n_{MG1} is the speed of motor MG1, T_{MG1} is the torque of motor MG1, and SOC is the battery state of charge.

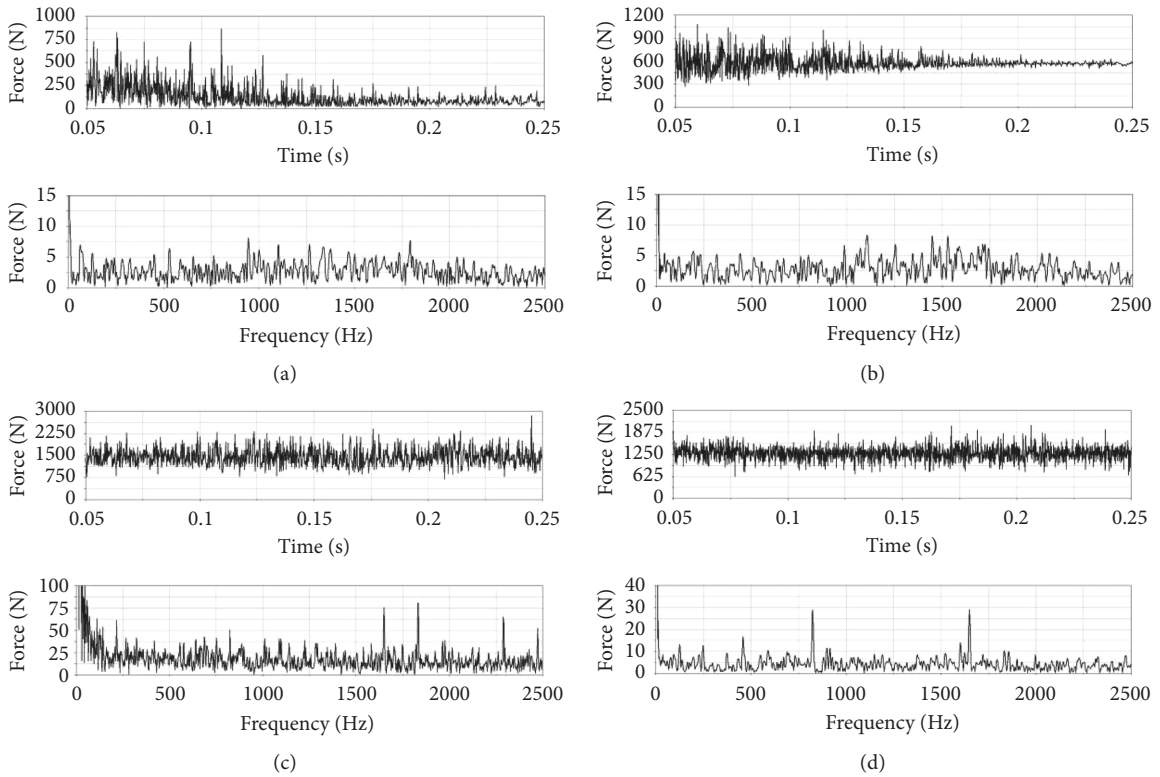

Figure 3: Continued.

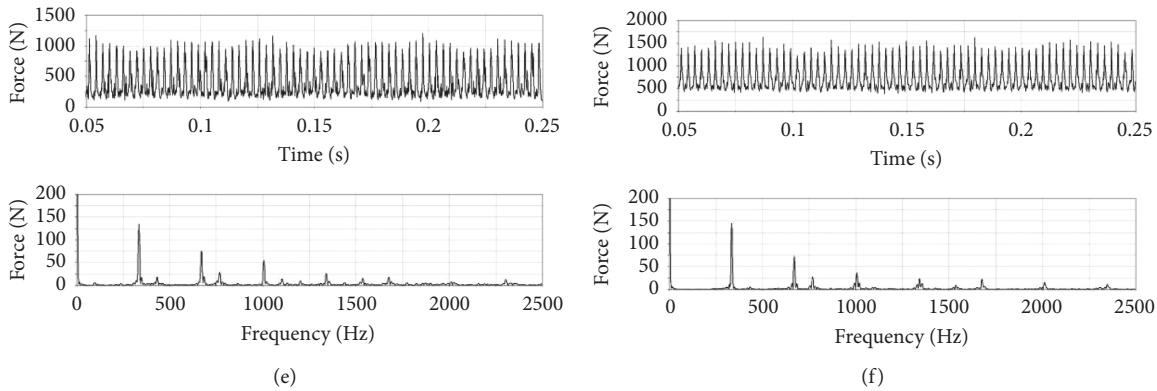

Figure 3: Time histories and frequency spectra of bearing constraining forces. (a) Engine input shaft bearing. (b) MG1 input shaft bearing. (c) Composite mechanism bearing. (d) MG2 input shaft bearing. (e) First reduction gear shaft bearing. (f) Second reduction gear shaft bearing.

the front planet row is switched, so its dynamic characteristics are quite complex. Figure 3(c) shows that the bearing constraining force of the composite mechanism shows some peaks at frequencies of 1650 Hz, 1830 Hz, 2280 Hz, and 2475 Hz, respectively. The related explanations are as follows: the calculation formula for gear-mesh frequency of planetary gear system is given by

$$f = \frac{(n_p - n_c)z_p}{60} = \frac{(n_s - n_c)z_s}{60} = \frac{(n_r - n_c)z_r}{60}, \quad (1)$$

where n_s, n_p, n_r, and n_c denote the speed of the sun gear, the planet gears, the internal gear ring, and the planet carrier separately. The z_s, z_p, and z_r denote the tooth number of the sun gear, the planet gears, and the internal gear ring.

Under the chosen working condition, the gear-mesh frequency of the rear planet row is 825 Hz according to Equation (1). The front planet row is in an unsteady state due to the power switching, so the gear-mesh frequency is uncertain. At the same time, the gear-mesh frequency of the first reduction gear assembly is 768 Hz. It can be seen that the 1650 Hz and 2475 Hz correspond to the double gear-mesh frequency and the three times gear-mesh frequency of the rear planet row, respectively, 2280 Hz is approximately equal to the three times gear-mesh frequency of the first reduction gear assembly (2304 Hz). The 1830 Hz is between 1650 Hz and 2304 Hz, so it is the result of the combined action of the front planet row, the rear planet row, and the first reduction gear assembly. Therefore, the peak frequencies of the composite mechanism are related to the gear-mesh frequencies of the front planet row, the rear planet row, and the first reduction gear assembly.

As shown in Figure 3(d), the bearing constraining force of MG2 input shaft shows some peaks at gear-mesh frequencies of the rear planet row (825 Hz and 1650 Hz, respectively). Although the power switching of the front planet row has a small impact on the bearings of the rear planet row, the operation of the rear planet row is stable.

In addition, the impact of the power switching from the front planet row on the reduction gear assembly is very small. It can be seen from Figures 3(e) and 3(f) that peaks in the frequency spectra appear at gear-mesh frequencies of the reduction gear assembly (335 Hz, 768 Hz, and their double frequencies, respectively).

4. Vibration Response Analysis of Power Coupling Mechanism Housing

4.1. Modelling of the Housing. With the help of software UG, the housing model of the power coupling mechanism is established, as shown in Figure 4. Then, the housing model is meshed with software ANSYS Workbench, and the unit size is 6 mm [13]. The finite element model of the housing is composed of 338402 units and 591466 nodes, as shown in Figure 5 below.

The housing is bolted to the frame. The degrees of freedom of the surface nodes at each fixed support are all constrained, as shown in Figure 6.

4.2. Vibration Response Analysis of the Housing. The modal superposition method [14] is used in harmonic response analysis of the housing. In order to calculate the vibration response of the housing under the load excitation with different frequencies, the bearing constraining forces obtained in Section 3 are applied to the housing through the spider-web structure. The analysis frequency range is 0–3000 Hz, and the step frequency is 10 Hz.

The vibration displacement response of housing surface when the frequencies are the first 10 natural frequencies of housing mode and the peak frequencies of the bearing constraining forces, respectively, is analysed and discussed. The results are as follows.

Firstly, since the excitation of gear-mesh and the thin-wall characteristics of housing itself, the maximum vibration displacement at each analysed frequency occurs mainly on the end cover of the front planet row, the end cover of the rear planet row, and the bearing seats of the front planet row housing. The vibration of the whole housing is mainly presented as the local deformation. The vibration displacement response at each analysed frequency is in good agreement with the excitation of the bearing constraining forces.

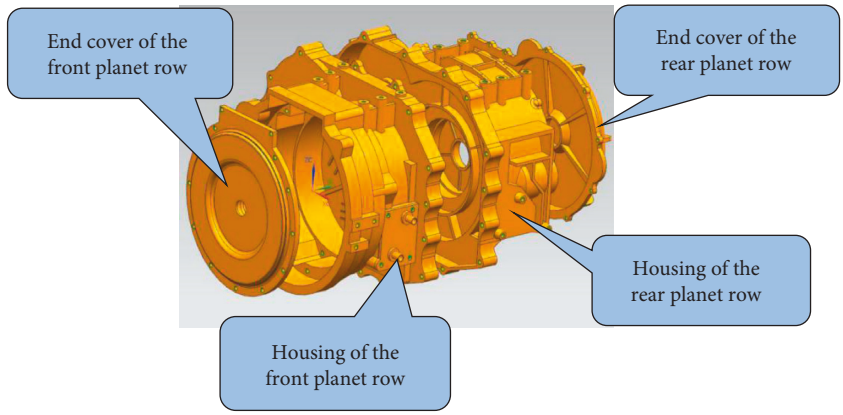

Figure 4: Housing of the power coupling mechanism.

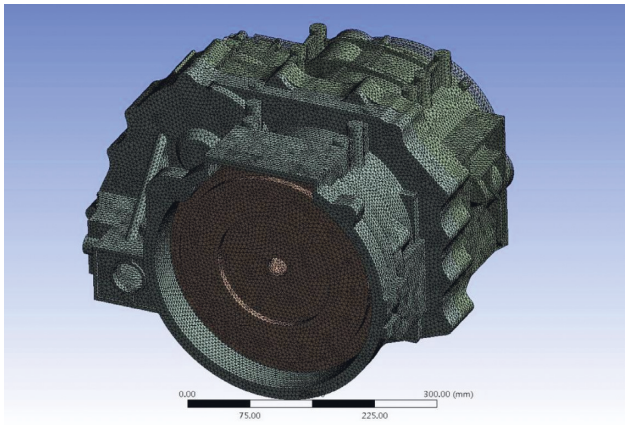

Figure 5: Finite element model of the housing.

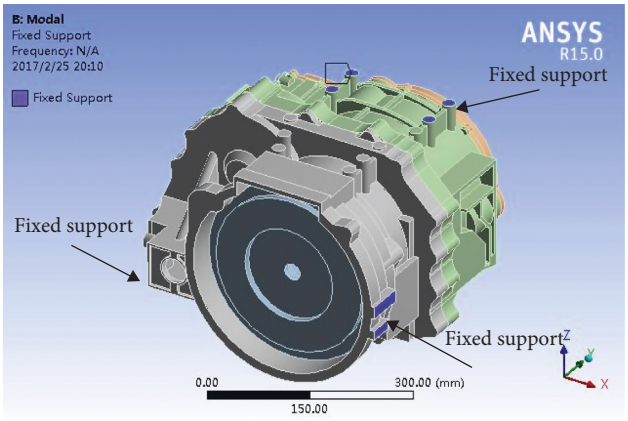

Figure 6: Fixed support of the housing.

Secondly, the maximum vibration displacement response of the end cover of the rear planet row appears in the third-order natural frequency (870 Hz), while the end cover of the front planet row obtains the maximum vibration displacement response when the frequency is the fourth-order natural frequency (1005 Hz), as shown in Figures 7(a) and 7(b).

5. Simulation and Analysis of the Housing Radiating Noise

5.1. Establishment of the Housing Acoustic Boundary Element Model. Acoustic boundary element method (BEM) is a commonly used method in acoustics calculation. Compared with the acoustic finite element method, it is more flexible and intuitive. In addition, the analytical method and numerical method are used comprehensively in the boundary element method, so this method has the advantages of low dimension, wide range, and high computational efficiency.

In this paper, the acoustic boundary element method is used with software LMS Virtual.Lab to simulate the housing radiating noise. The acoustic boundary element model of the housing is established with the software LMS Virtual.Lab, as shown in Figure 8. The size of acoustic mesh is 8 mm, and the model includes 10862 units and 10849 nodes.

5.2. Analysis of Simulation Results. In software LMS Virtual. Lab, the reference sound pressure is set as 2×10^{-5} Pa, the reference sound intensity is set as 1×10^{-12} W/m^2, the air density is set as 1.225 kg/m^3, and the sound velocity is set as 340 m/s. The vibration displacement response at the nodes of the housing surface in frequency domain is input to the acoustic boundary element model. The calculated frequency range is 200–3000 Hz, and the step frequency is 10 Hz. The frequency spectrum of radiating acoustic power is obtained and shown in Figure 9.

It can be seen from Figure 9 that the radiating acoustic power is bigger at the frequencies of 770 Hz, 870 Hz, 1010 Hz, 1650 Hz, and 2480 Hz. The 870 Hz and 1010 Hz correspond to the housing third- and fourth-order natural frequencies, 770 Hz corresponds to the meshing frequency of reduction gears, and 1650 Hz and 2480 Hz correspond to the double gear-mesh frequency and the three times gear-mesh frequency of the rear planet row, respectively.

Figure 10 illustrates the sound pressure level of the housing surface at every peak frequency of the radiating acoustic power spectrum. Because of the thin-wall characteristics and the lack of longitudinal bracing, the sound pressure level of housing surface is bigger on the front end

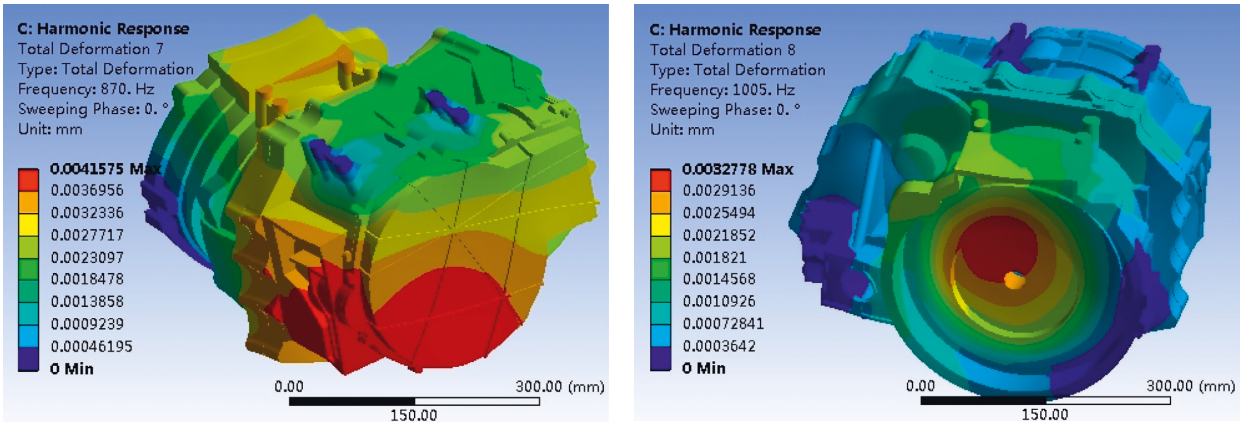

(a) (b)

Figure 7: Vibration response of the housing surface. (a) The 3rd natural frequency (870 Hz). (b) The 4th natural frequency (1005 Hz).

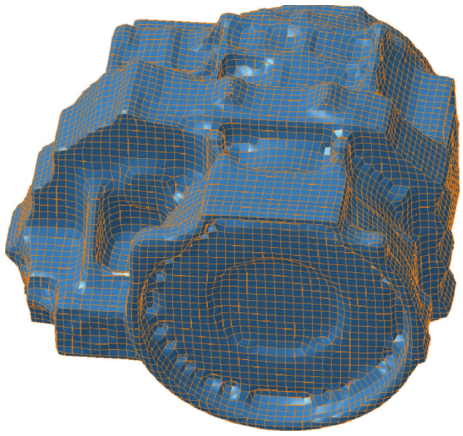

Figure 8: BEM model of the housing.

cover and the rear end cover. The maximum surface sound pressure level appears on the rear end cover when the frequency is 1650 Hz. At the same time, 1650 Hz is close to the double gear-mesh frequency of the rear planet row, so the gear-mesh of the rear planet row has a great influence on the radiating noise of the housing. At the same frequency, sound pressure level of the housing surface has a good correlation with the vibration displacement of surface.

5.3. Acoustic Contribution Analysis of Panels. The housing is divided into four acoustic panels, as shown in Figure 11. The front end cover and rear end cover correspond to panel 1 and panel 4, while the housing of the front planet row and the housing of the rear planet row correspond to panel 2 and panel 3, respectively.

In this paper, the acoustic contribution of each panel is calculated based on the approach of acoustic transfer vector (ATV). The range of calculated frequencies is 400–3000 Hz, and the step frequency is 10 Hz.

Figure 12 shows the color map of panel acoustic power contribution. It can be seen that panel 4 has the main contribution to the total radiating noise of housing. Therefore, the optimization of housing structure should give priority to the rear end cover.

6. Optimal Design of the Housing Structure

6.1. Mathematical Model of the Housing Optimization. It is suggested in acoustic contribution analysis of panels that the optimization of housing structure should give priority to the rear end cover. It is known that ribs can affect the vibration and radiating noise of a housing [15]. In order to improve the stiffness of the rear end cover, a new stiffener design is adopted here, as shown in Figure 13.

6.1.1. Design Variables. As shown in Figure 14, the free damping layer is selected to arrange on the rear end cover. The base layer thickness x_1, the damping layer thickness x_2, and the stiffener height x_3 are selected as design variables.

6.1.2. Constraint Conditions. Considering the function and rationality of the housing structure, following constraint conditions are given to the design variables x_1, x_2, and x_3:

$$\begin{aligned} 6 \le x_1 \le 8, \\ 2 \le x_2 \le 4, \\ 2 \le x_3 \le 10. \end{aligned} \tag{2}$$

Another constraint condition is that the mass M of the rear end cover after optimization cannot be more than the original mass M_0.

6.1.3. Objective Function. It is known from Section 5 that the housing radiating noise has a good correspondence with the vibration response. Therefore, the minimum value of the maximum normal vibration acceleration of each node on the housing surface is taken as the target to optimize the radiating noise. Theoretically, the more nodes are discussed, the more accurate the noise prediction is, but the larger the calculation scale is. In order to reduce the amount of computation, four typical nodes are selected from the finite

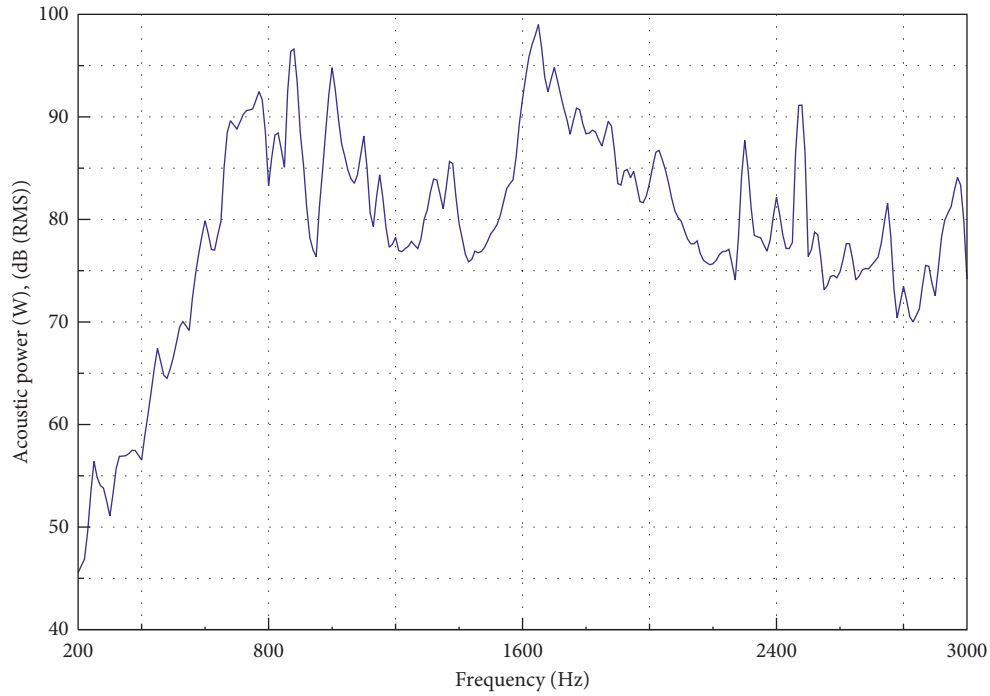

Plot	Set name	Name	Response name	Physical type	Function class	Data case	RPM	Order number	Argument physical type
——	Acousti response solution set.1	Real (model mesh:S)	(Model mesh:S)	Acoustic power	Frequency spectrum	Subcase 1			Frequency

Figure 9: Frequency spectrum of radiating acoustic power.

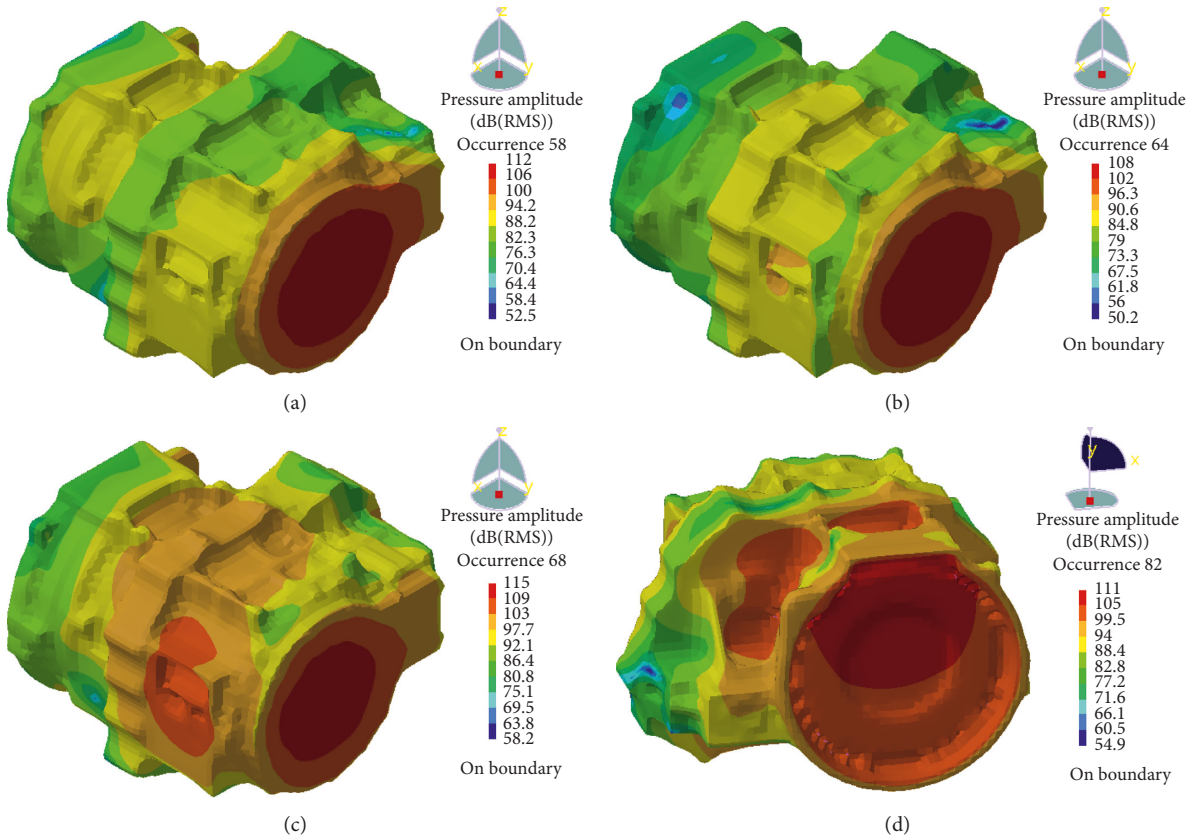

Figure 10: Continued.

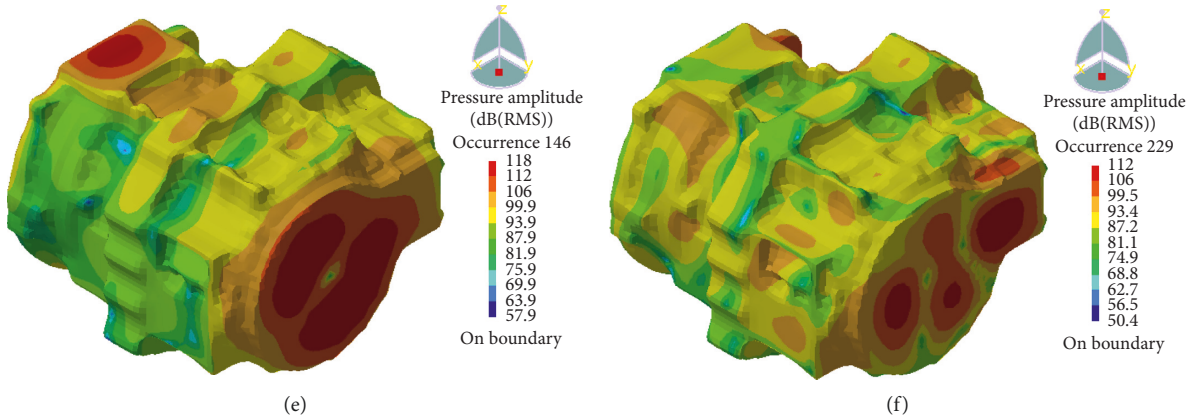

(e) (f)

Figure 10: Sound pressure levels of the housing surface. (a) 770 Hz. (b) 830 Hz. (c) 870 Hz. (d) 1010 Hz. (e) 1650 Hz. (f) 2480 Hz.

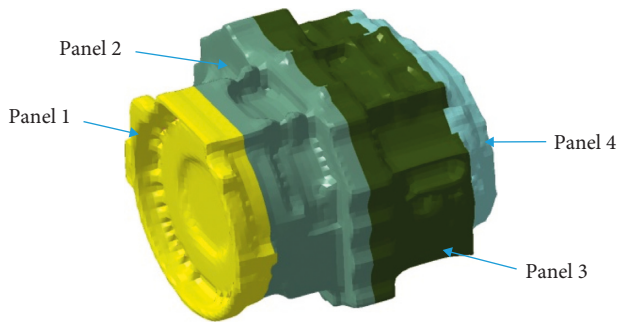

Figure 11: Panel division of the housing.

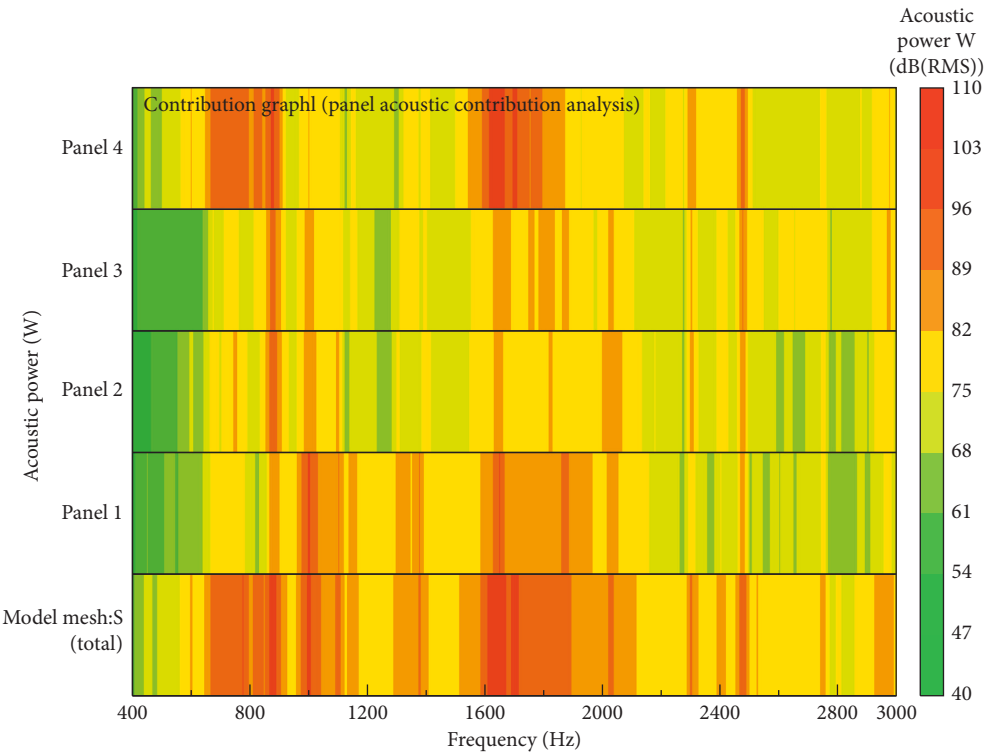

Plot	Set name	Name	Response name	Physical type	Function class	RPM	Order number
	Acousti response solution set.2	Color bars	(Model mesh:S)	Acoustic power	Frequency spectrum		

Figure 12: Color map of the panel acoustic power contribution.

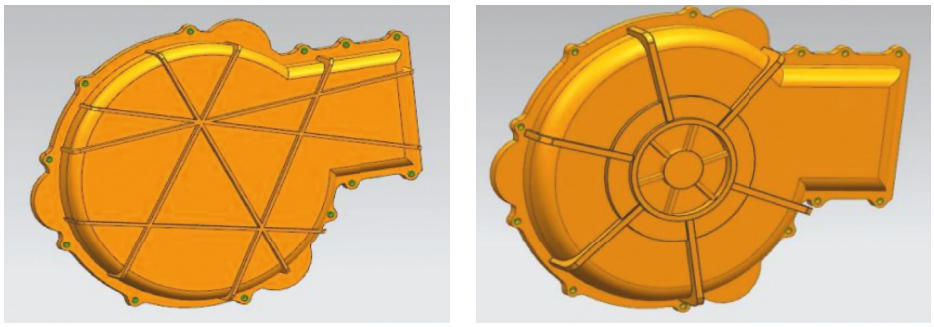

(a) (b)

Figure 13: Stiffener structure before and after optimization. (a) Before optimization. (b) After optimization.

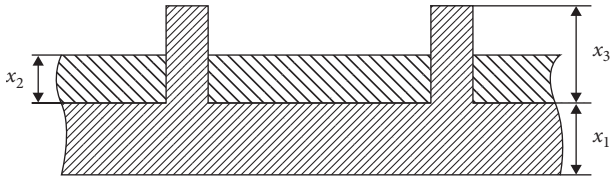

Figure 14: Structural design variables.

element model of the rear end cover, as shown in Figure 15. The maximum normal vibration accelerations of the 4 typical nodes are used to reflect the vibration characteristics of the whole rear end cover. So the expression of the objective function is given as

$$\max_{k=1\cdots4}(a_k) \longrightarrow \min, \tag{3}$$

where a_k is the maximum normal vibration accelerations of each typical node.

The K-S function is used to condense the maximum acceleration values of 4 typical nodes into a valid value which can reflect the vibration acceleration of the whole rear end cover. As a comprehensive index to describe the vibration characteristics of the whole rear end cover, this valid value can be written as

$$L_a = 20\log_{10}\frac{(1/p)\ln\sum_{j=1}^{n}e^{pa_j}}{a_0} = 20\log_{10}\frac{\ln\sum_{j=1}^{n}e^{pa_j}}{pa_0}, \tag{4}$$

where L_a is the vibration acceleration level; a_0 is the reference value of the vibration acceleration, $a_0 = 10^{-3}\,\mathrm{mm/s^2}$; a_j is the maximum normal vibration acceleration of node j; p is the stretching factor, $p = 4$ when solving structural problems; and n is the number of typical nodes, $n = 4$.

6.1.4. Optimization Model. Considering design variables, constraint conditions, and objective function, the optimization model of the rear end cover [16] is given by

$$\begin{cases} \min & L_a(x), \\ \text{s.t.} & M(x) \le M_0, \\ x_i^L \le x_i \le x_i^U & (i = 1,2,3). \end{cases} \tag{5}$$

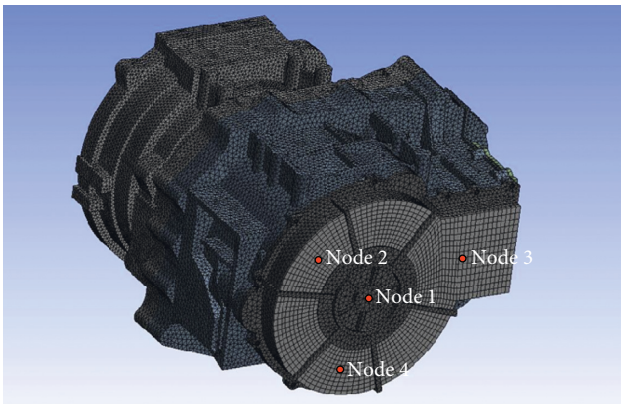

Figure 15: Locations of 4 typical nodes.

where $M(x) \le M_0$ is the mass constraint and $x_i^L \le x_i \le x_i^U$ $(i = 1,2,3)$ are dimension constraints.

6.2. Approximate Model of the Rear End Cover Response Surface. Response surface method (RSM) is a method for describing the relationship between input variables and response of complex systems by reasonably selecting test points and using a series of deterministic tests to fit the equation of state [17]. As a response surface method, the polynomial method has the advantages of simple mathematical expression, small calculation amount, fast convergence, and wide application in solving practical engineering problems. In theory, the higher the order of the polynomial, the more accurate the response surface model is, but the less efficient the calculation is. Therefore, considering the computational efficiency and the application characteristics of polynomial regression model, the quadratic polynomial is adopted in this paper to build the approximate model of the rear end cover response surface, and the expression is written as

$$L_a(\mathbf{x}) = \frac{1}{2}\mathbf{x}^T\mathbf{H}\mathbf{x} + \mathbf{c}^T\mathbf{x} + a_0. \tag{6}$$

Define

$$\mathbf{c} = \begin{pmatrix} a_1 \\ \vdots \\ a_n \end{pmatrix}_{n\times 1},$$
$$\mathbf{H} = \begin{pmatrix} a_{n+1} & 0 & \cdots & 0 \\ 0 & a_{n+2} & 0 & \vdots \\ \vdots & 0 & \ddots & 0 \\ 0 & \cdots & 0 & a_{n+n} \end{pmatrix}_{n\times n}, \tag{7}$$

where $n = 3$ and $\mathbf{x} = (x_1, x_2, x_3)$. Therefore, Equation (5) can be rewritten as

$$L_a(x_1, x_2, x_3) = a_0 + a_1x_1 + a_2x_2 + a_3x_3 + a_4x_1^2 + a_5x_2^2 + a_6x_3^2. \tag{8}$$

According to constraint conditions, $(x_1, x_2, x_3)^T = (7, 3, 6)^T$ is chosen as the central point and the fitting radius δ is taken as 0.5. In order to determine the 7 unknown coefficients in Equations (8) and (10), test points which are in the fitting radius are chosen as samples. For each sample, a new rear end cover will be established, and the vibration response of the housing with this new rear end cover will be obtained. The maximum acceleration values at 4 typical nodes will be used to calculate the vibration acceleration level L_a according to Equation (4). Finally, the vibration acceleration levels of 7 samples are shown in Table 4.

Although the expressions of Equations (4) and (8) are not in the same form, the values of the vibration acceleration level L_a obtained by them should be the same. Substituting the data of 7 samples in Equations (8) and (10), unknown coefficients will be calculated as

$$\begin{aligned} a_0 &= 225.467, \\ a_1 &= -2.980, \\ a_2 &= -31.404, \\ a_3 &= -1.869, \\ a_4 &= 0.124, \\ a_5 &= 4.368, \\ a_6 &= 0.074. \end{aligned} \tag{9}$$

Therefore, Equation (8) can be written as

$$L_a = 225.467 - 2.98x_1 - 31.404x_2 - 1.869x_3 + 0.124x_1^2 + 4.368x_2^2 + 0.074x_3^2. \tag{10}$$

In order to test the accuracy of the fitting function, the sample points in the range of design variables are randomly selected for special point test. Table 5 shows the relative errors between the fitting values obtained by Equation (10) and the simulation results obtained by Equation (4).

It can be seen from Table 5 that the error between the fitting value of acceleration level obtained by Equation (10) and the simulation result obtained by Equation (4) is less than 6%. Therefore, the fitting accuracy of the objective function derived from the response surface method is quite high, which can truly reflect the characteristics of the structure.

Table 4: Sample points and vibration acceleration levels.

Number	x_1 (mm)	x_2 (mm)	x_3 (mm)	L_a (dB)
1	7	3	6	147.233
2	6.5	3	6	147.886
3	7	2.5	6	148.703
4	7	3	5.5	147.742
5	7.5	3	6	146.642
6	7	3.5	6	145.727
7	7	3	6.5	146.761

6.3. Solution and Verification of the Optimization Model. Sequential quadratic programming (SQP) [18] is a programming problem with quadratic polynomial function as objective function and linear equality or inequality as constraint condition. Since the algorithm has high efficiency, good reliability, super linear convergence speed, and good numerical experimental results, it is used here to optimize the model.

6.3.1. Optimization Results. The optimization process starts with the initial value. The optimization process and data are shown in Table 6.

Figures 16 and 17 show the convergence process of the objective function value and the three design variables with the number of iterations.

From Figure 16, it can be seen that the value of the objective function tends to be stable when the iteration proceeds to the fourth step. When the iteration proceeds to the sixth step, L_a reaches the optimum.

Figure 17 shows that the three design variables tend to be stable from the fourth step. When the sixth step is carried out, the convergence condition of the variables is satisfied.

6.3.2. Verification of Optimization Effect. Based on the optimal solution of the optimization model, the acoustic boundary element model is reestablished. The radiating acoustic power level of the housing after optimization is calculated and compared with that before optimization, as shown in Figure 18.

The target problem of our study is to reduce the vibration and noise of the double planetary gear power coupling mechanism. In order to solve the target problem, we design a new rear end cover. It can be seen from Figure 18 that the optimization effect is obvious when the frequencies are between 700 Hz and 900 Hz or near 1650 Hz. When the frequency is 1650 Hz corresponding to the maximum acoustic power, the optimized acoustic power level is decreased by 5.59 dB. Meanwhile, the acoustic power level is decreased by 3.94 dB at 770 Hz, decreased by 3.92 dB at 870 Hz, and decreased by 2.84 dB at 2480 Hz after optimization. Therefore, the optimization effect is obvious in reducing the vibration and radiating noise of the housing.

Table 5: Comparison of fitting values and simulation results.

Special points	Fitting values (dB)	Simulation results (dB)	The relative errors (%)
$(6, 3, 6)^T$	148.601	143.645	+3.45
$(6, 4, 4)^T$	150.031	143.214	+4.76
$(7, 2, 4)^T$	159.055	152.717	+4.15
$(7, 4, 6)^T$	146.405	150.762	−2.89
$(8, 4, 6)^T$	145.285	139.536	+4.12
$(8, 4, 8)^T$	143.619	136.196	+5.45

Table 6: Results of each iteration.

Iterative step	x_1 (mm)	x_2 (mm)	x_3 (mm)	Target value L_a (dB)
0	7.0000	3.0000	6.0000	147.2330
1	6.1039	4.0000	6.8156	146.8684
2	6.2398	3.5657	7.6846	145.2662
3	6.1890	3.4263	9.1849	144.5284
4	6.1085	3.4639	10.0000	144.2302
5	6.0870	3.5098	10.0000	144.2184
6	6.0841	3.5160	10.0000	144.2183

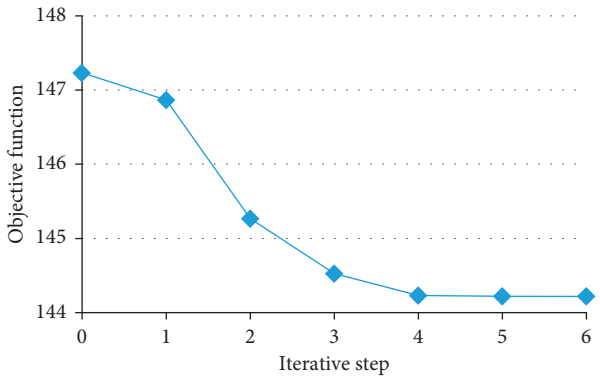

Figure 16: Iterative process of objective function.

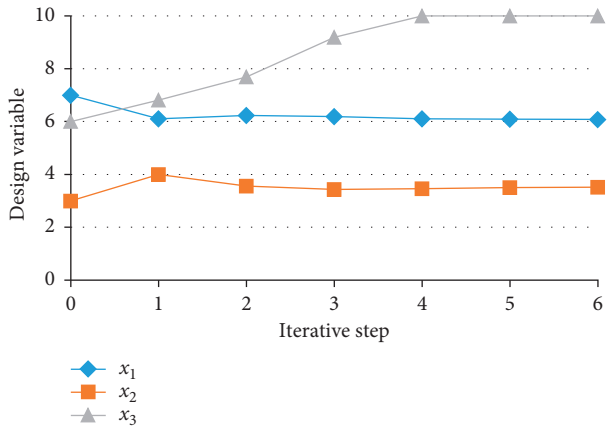

Figure 17: Iterative process of design variables.

7. Conclusions

In this paper, the vibration response and radiating noise of the power coupling mechanism housing are analysed and discussed. At the same time, an optimization model of the housing rear end cover is established and solved to obtain the optimal structure of the housing. The main conclusions can be summarized as follows:

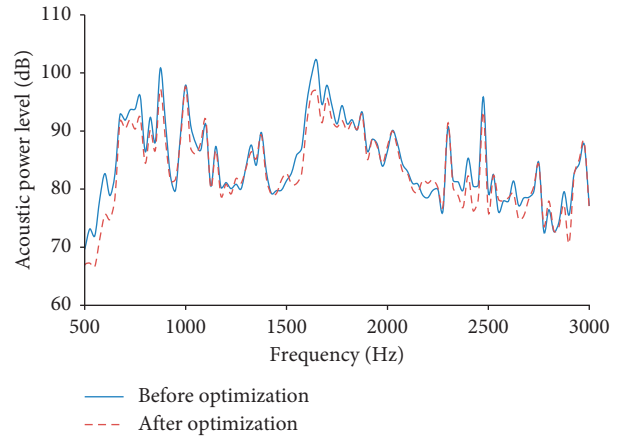

Figure 18: Acoustic power level before and after optimization.

(1) The vibration of the whole housing is mainly presented as local deformation. The maximum vibration displacement of the front end cover appears at the fourth-order natural frequency (1005 Hz), while the rear end cover has bigger vibration displacement when the frequencies are 768 Hz, 870 Hz, and 1650 Hz, respectively. The vibration response of the whole housing surface is in good accordance with the excitation of the bearing constraining forces.

(2) The housing radiating noise has a good correspondence with the vibration response. The radiating acoustic power of the housing is bigger when the frequencies are 770 Hz, 870 Hz, 1010 Hz, 1650 Hz, and 2480 Hz, respectively. At the same time, based on the approach of acoustic transfer vector, the acoustic contributions of four panels of the housing are analysed, and the rear end cover (panel 4) is found to have the largest acoustic contribution.

(3) The housing acoustic power level after optimization is decreased by 3.94 dB at 770 Hz, decreased by 3.92 dB at 870 Hz, decreased by 5.59 dB at 1650 Hz, and decreased by 2.84 dB at 2480 Hz. Therefore, the optimization effect is obvious in reducing the vibration and radiating noise of the power coupling mechanism housing.

Data Availability

The data used to support the findings of this study are available from the corresponding author upon request.

Conflicts of Interest

The authors declare that there are no conflicts of interest regarding the publication of this paper.

Acknowledgments

This work was financially supported by National Natural Science Foundation of China (51575238).

References

[1] S. L. Han, S. Feng, and J. Zhao, "Motion state and transient analysis of the hybrid power coupling mechanism based on matlab and solidworks," in *Proceedings of the Second International Conference on Mechatronics and Automatic Control*, pp. 229–236, Springer International Publishing, Cham, Switzerland, August 2015.

[2] D. Popa, S. Pârlac, and N. D. Stănescu, "The study of the vibrations and noises of a stand with planetary mechanism used in the power sources coupling," *Romanian Journal of Acoustics and Vibration*, vol. 10, no. 2, pp. 97–102, 2013.

[3] F. T. Zhu, L. Chen, and C. Yin, "Scheme design and optimal selection for HEV planetary gear coupling mechanism," in *Proceedings of ASME International Design Engineering Technical Conferences/Computers and Information in Engineering Conference*, pp. 943–949, San Diego, CA, USA, 2009.

[4] T. Eritenel and R. G. Parker, "An investigation of tooth mesh nonlinearity and partial contact loss in gear pairs using a lumped-parameter model," *Mechanism and Machine Theory*, vol. 56, no. 1, pp. 28–51, 2012.

[5] H. Optiz, "Dynamic behavior of spur and helical gears," in *Proceedings of JSME Semi-International Symposium Papers*, pp. 199–209, Tokyo, Japan, September 1967.

[6] A. Kahraman, "Effect of axial vibrations on the dynamic of helical gear pairs," *ASME Journal of Vibration and Acoustics*, vol. 115, no. 1, pp. 33–38, 1993.

[7] A. Kahraman, "Dynamic analysis of a multi-mesh helical gear train," *ASME Journal of Mechanical Design*, vol. 116, no. 1, pp. 706–712, 1994.

[8] A. Kahraman, "Natural modes of planetary gear trains," *Journal of Sound and Vibration*, vol. 173, no. 1, pp. 123–132, 1994.

[9] T. J. Lin, H. Ou, and R. Li, "A finite element method for 3D static and dynamic contact/impact analysis of gear drives," *Computer Methods in Applied Mechanics and Engineering*, vol. 196, no. 9–12, pp. 1716–1728, 2007.

[10] W. Shabbir and S. A. Evangelou, "Real-time control strategy to maximize hybrid electric vehicle powertrain efficiency," *Applied Energy*, vol. 135, pp. 512–522, 2014.

[11] Y. T. Luo and Y. Chen, "Dynamic modeling and analysis of power coupling system with two-stage planetary gear trains for hybrid system," *Journal of Mechanical Engineering*, vol. 48, no. 5, pp. 70–75, 2012.

[12] S. P. Fu, C. L. Xiang, and S. W. Yao, "Analysis for dynamics simulation of rigid- flexible coupling gear transmission in consideration of flexible bearing," *Journal of Shanghai Jiaotong University*, vol. 44, no. 4, pp. 495–499, 2010.

[13] C. M. Chu, Y. H. Du, B. Zhang et al., "A research on optimal mesh generation in finite element analysis for transmission housing," *Automotive Engineering*, vol. 36, no. 7, pp. 885–889, 2014.

[14] Z. P. Mourelatos, "A crankshaft system model for structural dynamic analysis of internal combustion engines," *Computers and Structure*, vol. 79, no. 20-21, pp. 2009–2027, 2001.

[15] S. L. Moyne and J. L. Tebec, "Ribs effects in acoustic radiation of a gearbox—their modelling in a boundary element method," *Applied Acoustics*, vol. 63, no. 2, pp. 223–233, 2002.

[16] Z. Y. He, T. Lin, and T. Lui, "Arborne noise optimization design of gear system," *Noise Control Engineering Journal*, vol. 64, no. 2, pp. 115–125, 2016.

[17] W. J. Roux, N. Stander, and R. T. Haftka, "Response surface approximations for structural optimization," *International Journal for Numerical Method in Engineering*, vol. 42, no. 3, pp. 517–534, 2015.

[18] J. B. Etoa, "Solving convex quadratic bilevel programming problems using an enumeration sequential quadratic programming algorithm," *Journal of Global Optimization*, vol. 47, no. 4, pp. 615–637, 2010.

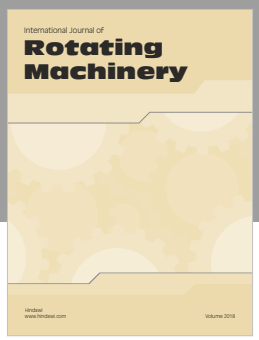

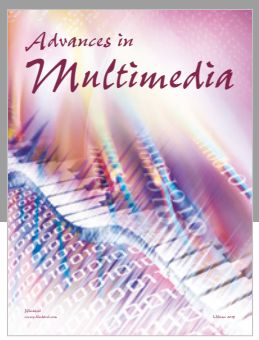

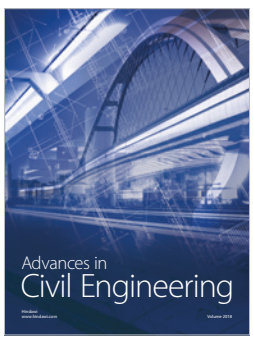

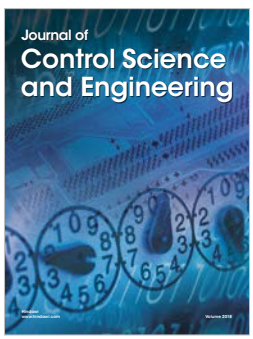

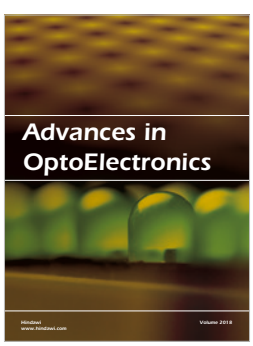

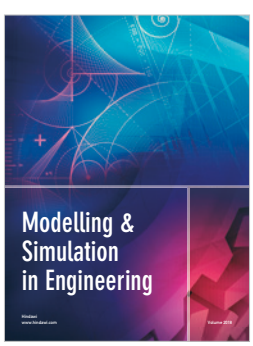

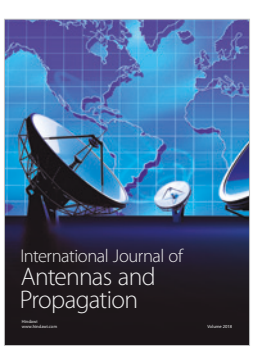

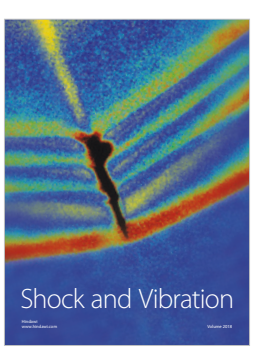

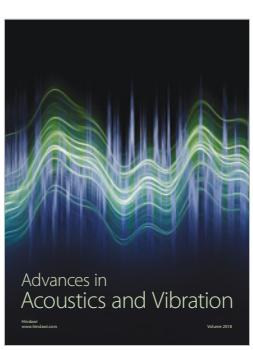

Hindawi

Submit your manuscripts at
www.hindawi.com